typeset using JPSJ.sty <ver.1.0b>

# Theoretical Temperature-Pressure Phase Diagram for $\{N(CH_3)_4\}_2ZnCl_4$

Daniil G. Sannikov, Grigorii A. Kessenikh
and Hiroyuki Mashiyama[1]

*Institute of Crystallography, Russian Academy of Sciences, Moscow 117333, Russia*
[1]*Department of Physics, Yamaguchi University, Yamaguchi 753-8512*

(Received July 28, 1999)

A phenomenological approach for construction theoretical phase diagrams with multiple phase transitions including incommensurate transitions is developed for the case when a special triple point, a Lifshitz-type point, is assumed to be present in the experimental diagram for $\{N(CH_3)_4\}_2ZnCl_4$ crystal family. The theoretical temperature-pressure phase diagram for $\{N(CH_3)_4\}_2ZnCl_4$ is plotted and is found to be in agreement with the experimental phase diagram. The approximations and assumptions made in the construction of the diagrams are discussed.

KEYWORDS: T-P phase diagram, incommensurate, ferroelectrics, TMATC-Zn compound

## §1. Introduction

Tetramethylammonium (TMA) tetrachlorometallic compounds, $\{N(CH_3)_4\}_2MCl_4$ (abbreviated TMATC-$M$, hereafter) , where $M$ stands for divalent metals (Mn, Zn, Fe, Co, etc.) and H can be replaced by D, are well studied crystals with incommensurate phase (IC phase) and many commensurate phases ($C_{m/l}$ phases).[1–3)] The temperature-pressure, T-P, phase diagrams were first obtained for TMATC-$M$ by Shimizu *et al.*[4,5)] Figure 1 schematically shows the unified T-P phase diagram, which represents the form of T-P phase diagrams for all the crystal family if temperature and pressure are scaled and their origins are shifted properly.

According to experimental data (see ref. 1–3 and references cited therein), the space group $D_{2h}^{16}$ of the initial prototype phase is $Pmcn$. The modulation wave vector of the IC phase is $k_z = qc^*$. Space groups of the $C_{m/l}$ phases with different dimensionless wavenumbers $q_{m/l} = m/l$ are the following:[6,7)] $q_{0/1}$ - $C_{2h}^5$ ($P12_1/c1$), $q_{1/3}$ - $C_{2h}^5$ ($P112_1/n$), $q_{3/7}$ - $D_2^4$ ($P2_12_12_1$), $q_{2/5}$ - $C_{2v}^9$ ($P2_1cn$), $q_{1/2}$ - $C_{2h}^5$ ($P2_1/c11$), and $q_{1/3}$ - $D_2^4$ ($P2_12_12_1$).

The aim of this paper is to develop a phenomenological approach for construction of the T-P phase diagrams for the considered crystal family. As an example we choose TMATC-Zn, since the

experimental T-P phase diagram shown in Fig. 2 of ref. 8 is comparatively simple: the number of $C_{m/l}$ phases is small. First we construct a phase diagram in dimensionless variables $D$ and $A$, which are combinations of coefficients of thermodynamic potential. Assuming a linear dependence of $D$ and $A$ on temperature and pressure, we can present the theoretical T-P phase diagram and compare it with the experimental diagram.

Note that phenomenological approaches describing the phase transition sequence in TMATC-Zn have been previously applied in many papers,[9] however, those approaches differ from the present simple model. In particular, so far the theoretical T-P phase diagram was not constructed.

The main problem in a phenomenological approach is to obtain the thermodynamic potentials for all of the possible phases in TMA-family crystals. For this purpose we combine two different approaches to the description of IC phase transitions. The first one provides thermodynamic potentials for the IC and $C_{m/l}$ phases (with the exception of the phase $C_{0/1}$ with $q = 0$). The second one gives the potentials for the IC and $C_{0/1}$ phases. Both approaches have to provide precisely the same expression for the IC phase potential. Thus the thermodynamic potentials for all the phases are obtained with self-consistent coefficients.

It seems to be reasonable that all phases observed in the TMATC-$M$ family crystals are due to a single soft optical branch of the spectrum of normal modes of the prototype phase of the crystals.[8] The language of lattice dynamics is useful regardless of whether the phase transitions under investigation are of displacive or order-disorder type. The space groups of the $C_{m/l}$ phases are in agreement with this assumption (see Table I). The symmetry of this branch is unambiguously determined by the space group $P12_1/c1$ ($C_{2h}^5$) of the $C_{0/1}$ phase provided that the prototype phase ($C_0$) is $Pmcn$ ($D_{2h}^{16}$), and the wave vector of the IC phase is directed along the $z$-axis.

Table I, which is extraction from tables of ref. 10, gives the space groups for all possible $C_{m/l}$ phases corresponding to this branch (see also the table in ref. 6, where the soft branch under consideration was first considered to be responsible for all the phases observed in TMATC-Zn). The first column of the table gives the representation of the point group $mmm$ ($D_{2h}$), according to which the transition into the $C_{0/1}$ phase occurs. In the parentheses the lower-rank tensor component is given which transforms according to this representation. The space group of the $C_{0/1}$ phase is also given. The following three columns give the space groups of three possible phases $c_1$, $c_2$ and $c_3$ for each $C_{m/l}$ phase for all $q_{m/l} = m/l$ ($m_+$, $l_+$ are even integers and $m_-$, $l_-$ are odd integers). Spontaneous values for lower-rank tensor components in phases $c_1$ and $c_2$ are also given (for details, see ref. 10).

## §2. Thermodynamic Potentials

We proceed from the assumption that the triple point between the $C_0$, IC and $C_{0/1}$ phases denoted by the letters LT in the phase diagrams (Figs. 1 and 2 ) is the special point which was theoretically introduced by Aslanyan and Levanyuk.[11] Although it was called as L-point by analogy with the

Lifshitz point,[12] we call it Lifshitz-type (LT) point because its properties differ from that of the L-point (see a classification of such triple points in ref. 13 ).

According to this assumption, we represent the soft optical branch or, more precisely, a dependence of the elastic coefficient $\alpha$ on the wavenumber $q$ by the expression

$$\alpha(q) = \alpha - \delta q^2 - \kappa q^4 + \tau q^6, \tag{1}$$

where $\kappa > 0$ and $\tau > 0$ are supposed. Above equation can be rewritten in the form

$$\alpha(q) = a + \tau(b^2 - q^2)^2[2(b^2 - q_L^2) + q^2], \tag{2}$$
$$a = \alpha - 2\tau b^4(b^2 - q_L^2), \quad \delta = \tau b^2(3b^2 - 4q_L^2), \quad q_L^2 = \kappa/2\tau,$$

where we introduce two new variables $a$ and $b$ and the notation $q_L$.

According to the symmetry of the $C_0$ phase, any optical branch has a fixed extremum only in the center of the Brillouin zone. This extremum, equal to $\alpha(0) = \alpha$, is a minimum if $\delta < 0$ and is a maximum if $\delta > 0$. From eq. (1), under the condition $\delta > -\frac{\kappa^2}{3\tau}$, it follows that $\alpha(q)$ has a minimum at an arbitrary point of the Brillouin zone:

$$q = b, \qquad \alpha(b) = a. \tag{3}$$

where $b$ is the position and $a$ is the value of this minimum. Thus, in the interval of values $-\kappa^2/3\tau < \delta < 0$, the dependence $\alpha(q)$ has two minima. Their values become equal to each other $\alpha = a$ at $\delta = -\kappa^2/4\tau$ or $b = q_L$. When $\alpha = a = 0$, the coordinates of the LT-point on the ($\delta$, $a$) plane[11] and on the ($b$, $a$) plane are determined, respectively, by:

$$\delta = -\tau q_L^4, \quad a = 0; \quad b = q_L, \quad a = 0. \tag{4}$$

The soft mode expressed by the dependence $\alpha(q)$ is doubly degenerate, i.e. $\alpha(q) = \alpha(-q)$. Hence, the star of wave vectors has two rays and the order parameter corresponding to an arbitrary $q$-value has two components. The components $\eta$ and $\xi$ can be regarded as amplitudes of two modes with wavenumbers $q$ and $-q$ which belong to this branch. Using the polar coordinate system $\eta = \rho\ \cos\varphi$ and $\xi = \rho \sin\varphi$, we can write the thermodynamic potential in the form[14]

$$\Phi = \alpha(q)\rho^2 + \beta\rho^4 - \alpha'_{2l}\rho^{2l}\ \cos 2l\varphi, \tag{5}$$

where $\alpha(q)$ is given by eq. (1) or (2). We suppose that the coefficients $\beta$ and $\alpha'_{2l}$ are independent of $q$, and $\beta > 0$. We neglect invariants higher orders in $\rho$, in particular, those that are necessary for $\Phi$ being not equal to $-\infty$ at $\rho = \infty$. Note that invariants of higher orders in $\rho$ do not change the results substantially. The coefficient $\alpha'_{2l}$ of the anisotropic (in the $\eta - \xi$ space) invariant is nonzero only for rational values $q = q_{m/l} = m/l$, where $m$ and $l$ are integers.

For the IC phase $q$ has irrational values, and the potential takes the form

$$\Phi_{\rm IC} = (\alpha - \delta q^2 - \kappa q^4 + \tau q^6)\rho^2 + \beta\rho^4. \tag{6}$$

Since the mode with given $q$ is harmonic vibration, we can say that expression (6) is obtained in a single-harmonic approximation.

In the approach discussed above, which can be called a phenomenological description of a devil's staircase,[14] it is impossible to obtain the $C_{0/1}$ phase potential, since the soft branch at the point $q = 0$ is nondegenerate, i.e. only one mode corresponds to the value $q = 0$ (all the irreducible representations of the point group $D_{2h}$ are one-component). Therefore we use the approach to description of the $C_0$-IC-$C_{0/1}$ phase transition sequence.[15] The density of thermodynamic potential can be presented in the form

$$\Phi(z) = \alpha\zeta^2 + \beta\zeta^4 - \delta(\frac{\partial\zeta}{\partial z})^2 - \kappa(\frac{\partial^2\zeta}{\partial z^2})^2 + \tau(\frac{\partial^3\zeta}{\partial z^3})^2, \tag{7}$$

where $\zeta$ is a one-component order parameter which can be considered as the amplitude of the mode with $q = 0$ belonged to the same soft branch. The spatial coordinate $z$ is scaled by the lattice parameter $c$.

In a single harmonic approximation,

$$\zeta = \sqrt{2}\rho\ \cos qz, \tag{8}$$

the potential of the IC phase, according to eq. (7), takes the form

$$\Phi_{\rm IC} = (\alpha - \delta q^2 - \kappa q^4 + \tau q^6)\rho^2 + \frac{3}{2}\beta\rho^4. \tag{9}$$

For the same IC phase the potential in the first approach, i.e. in the notation of eq. (5), has the form of eq. (6). The potentials (9) and (6) will be equivalent if we replace in eq. (9) $\frac{3}{2}\beta$ by $\beta$. The same replacing must be made in eq. (7) for the potential of the $C_{0/1}$ and $C_0$ phases:

$$\Phi_{0/1} = \alpha\zeta^2 + \frac{2}{3}\beta\zeta^4. \tag{10}$$

Thus, using two different phenomenological approaches for the description of IC phase transitions, and requiring that they must provide the same expressions for the potential of the IC phase in both approaches, we have obtained the thermodynamic potentials for all of the possible phases in TMATC-$M$; namely eq. (5) for the $C_{m/l}$ phases, eq. (6) for the IC phase, and eq. (10) for the $C_{0/1}$ and $C_0$ phases.

## §3. Minimization of the Thermodynamic Potentials

We now minimize these potentials with respect to their variables to simplify them as far as possible. Minimizing eq. (10) with respect to $\zeta$, we obtain the values of thermodynamic potentials for the $C_0$ phase ($\alpha > 0$) and $C_{0/1}$ phase ($\alpha < 0$), respectively

$$\Phi_0 = 0, \quad \Phi_{0/1} = -3\alpha^2/8\beta. \tag{11}$$

Minimizing eq. (6) with respect to $q$, we obtain the equilibrium value of $q$, which has been given above: $q = 0$, $\alpha(0) = \alpha$ at $\delta < -\kappa^2/4\tau$, or $b < q_L$, and eq. (3) at $\delta > -\kappa^2/4\tau$, or $b > q_L$. Next minimizing eq. (6) with respect to $\rho$, we arrive at the expression

$$\Phi_{\rm IC} = -a^2/4\beta, \tag{12}$$

at $a < 0$ and $b > q_L$. Note that $\Phi_{\rm IC} = -\alpha^2/4\beta$ at $\alpha < 0$ and $b < q_L$, which value is larger than the value of $\Phi_{0/1}$ in eq. (11), and, hence, the IC phase is unstable at $b < q_L$.

The $C_{m/l}$ phases are characterized by the fixed numbers $q_{m/l} = m/l$. Minimizing eq. (5) with respect to $\varphi$, we obtain $\cos 2l\varphi = \pm 1$, that corresponds to the phases $c_1$ and $c_2$ (for each $C_{m/l}$ phase, see Table I), which are stable for $\alpha'_{2l} > 0$ and $< 0$, respectively. Now minimizing eq. (5) with respect to $\rho$, we arrive at the expression

$$\Phi_{m/l} = -\frac{\alpha^2_{m/l}}{4\beta}[1 + \frac{|\alpha'_{2l}|}{\beta}(\frac{-\alpha_{m/l}}{2\beta})^{l-2}], \tag{13}$$
$$\alpha_{m/l} \equiv \alpha(q_{m/l}),$$

which is valid at the condition of weak anisotropy. This condition implies that the anisotropic (i.e. $\varphi$-dependent) invariant in potential (5) is small in comparison with isotropic (independent of $\varphi$) invariant:

$$\frac{|\alpha'_{2l}|\rho^{2l}}{2\beta\rho^4} = \frac{|\alpha'_{2l}|}{2\beta}(\frac{-\alpha_{m/l}}{2\beta})^{l-2} \ll 1, \tag{14}$$

For $l = 2$ the condition (14) is not fulfilled, but we can obtain an explicit expression for the potential without resorting to the condition of weak anisotropy:

$$\Phi_{1/2} = -\frac{\alpha^2_{1/2}}{4(\beta - |\alpha'_4|)}, \tag{15}$$

where $|\alpha'_4| < \beta$ is assumed.

## §4. Phase Boundaries

Equating the thermodynamic potentials for different phases, i.e. eqs. (11)-(13) and (15), we obtain expressions for the boundaries between phases, i.e. lines of phase transitions. It is useful to introduce the following variables and parameters:

$$D = \frac{\delta}{\tau Q^4}, \qquad A = -\frac{a}{\tau Q^6}, \qquad B = \frac{b}{Q},$$
$$Q_{m/l} = \frac{q_{m/l}}{Q}, \qquad Q_L = \frac{q_L}{Q}, \qquad \epsilon_{2l} = \frac{\tau Q^6}{2\beta}(\frac{|\alpha'_{2l}|}{\tau Q^6})^{1/(l-1)}. \tag{16}$$

For convenience the sign of $A$ is chosen opposite to that of $a$. Each $C_{m/l}$ phase is characterized by only one dimensionless parameter $\epsilon_{2l}$ depending on the magnitude of the coefficient $\alpha'_{2l}$. $Q$ is simply a number and we introduce it in eq. (16) only for convenience of choosing different values during the calculation of phase diagrams.

First we construct a phase diagram in the plane of $D$ and $A$, choosing these variables as coordinate axes and setting $Q_L$ and $\epsilon_{2l}$ being constant. From eq. (12) the $C_0$-IC boundary is given by

$$A = 0. \tag{17}$$

For the IC-$C_{m/l}$ boundary we obtain from eqs. (12) and (13) under the condition (14) the expression

$$A = \frac{1}{\epsilon_{2l}}\{(B^2 - Q_{m/l}^2)^2[2(B^2 - Q_L^2) + Q_{m/l}^2]\}^{1/(l-1)}. \tag{18}$$

The condition of weak anisotropy (14) is reduced to the form

$$\epsilon_{2l}(\epsilon_{2l}A)^{l-2} \ll 1. \tag{19}$$

For the $C_{m/l}$-$C_{m'/l'}$ boundary we obtain from (13) under the condition (19) the expression

$$\begin{aligned}(\epsilon_{2l}A)^{l-1} - (B^2 - Q_{m/l}^2)^2[2(B^2 - Q_L^2) + Q_{m/l}^2] \\ = (\epsilon_{2l'}A)^{l'-1} - (B^2 - Q_{m'/l'}^2)^2[2(B^2 - Q_L^2) + Q_{m'/l'}^2],\end{aligned} \tag{20}$$

which can be resolved with respect to $B^2$.

We consider the boundaries with the $C_{0/1}$ phase. The $C_0$-$C_{0/1}$ boundary, as follows from eq. (11), has the form

$$A = 2B^4(B^2 - Q_L^2). \tag{21}$$

The IC-$C_{0/1}$ boundary, as follows from (12) and (11), has the form

$$A = 2c_0B^4(B^2 - Q_L^2), \qquad c_0 \equiv 3 + \sqrt{6} \simeq 5.45. \tag{22}$$

For the $C_{0/1}$-$C_{m/l}$ boundary we obtain from (13) and (11) under the condition (19) the expression

$$\begin{aligned}A = 2c_0B^4(B^2 - Q_L^2) - (c_0 - 1)(B^2 - Q_{m/l}^2)^2[2(B^2 - Q_L^2) + Q_{m/l}^2] \\ +(c_0 - 1)(\epsilon_{2l}A)^{l-1}.\end{aligned} \tag{23}$$

We consider the boundaries with the $C_{1/2}$ phase. The IC-$C_{1/2}$ boundary, as follows from (12) and (15), has the form

$$\begin{aligned}A = c_4(B^2 - Q_{1/2}^2)^2[2(B^2 - Q_L^2) + Q_{1/2}^2], \\ c_4 \equiv \frac{1}{2\epsilon_4}[1 + (1 - 2\epsilon_4)^{1/2}], \quad \epsilon_4 = \frac{|\alpha_4'|}{2\beta}.\end{aligned} \tag{24}$$

For the $C_{m/l}$-$C_{1/2}$ boundary we obtain from (13) and (15) under the condition (19) the expression

$$\begin{aligned}A = c_4(B^2 - Q_{1/2}^2)^2[2(B^2 - Q_L^2) + Q_{1/2}^2] \\ -(c_4 - 1)(B^2 - Q_{m/l}^2)^2[2(B^2 - Q_L^2) + Q_{m/l}^2] + (c_4 - 1)(\epsilon_{2l}A)^{l-1}.\end{aligned} \tag{25}$$

The $C_{0/1}$-$C_{1/2}$ boundary, as follows from (15) and (11), has the form

$$A = (c_4 - c_0)^{-1}\{c_0(c_4 - 1)2B^4(B^2 - Q_L^2) - c_4(c_0 - 1)(B^2 - Q_{1/2}^2)^2[2(B^2 - Q_L^2) + Q_{1/2}^2]\}. \tag{26}$$

The boundaries $C_0$-IC, eq. (17), $C_0$-$C_{0/1}$, eq. (21), and IC-$C_{0/1}$, eq. (22), intersect at the LT-point. Its coordinates are

$$D = -Q_L^4, \qquad A = 0. \tag{27}$$

These three boundaries converge to the LT-point at angles to each other, and the value of $q$ changes by jump to zero at the LT-point. Therein lies the difference between the LT-point and the Lifshitz-point. The boundaries IC-$C_{m/l}$, IC-$C_{m'/l'}$, eq. (18), and $C_{m/l}$-$C_{m'/l'}$, eq. (20), intersect at a single point. This is also the case for boundaries IC-$C_{m/l}$, eq. (18), IC-$C_{0/1}$, eq. (22), and $C_{0/1}$-$C_{m/l}$, eq. (23), as well as for the boundaries IC-$C_{m/l}$, eq. (18), IC-$C_{1/2}$, eq. (24), and $C_{m/l}$-$C_{1/2}$, eq. (25). These intersections confirm the fact that none of the expressions for the boundaries contain terms which are beyond the accuracy of the approach determined by condition (19).

Expression (2), connecting $\delta$ and $b^2$, takes the form

$$D = B^2(3B^2 - 4Q_L^2). \tag{28}$$

Note that the variables $D$ and $A$ are expressed in terms of $B^2$. Therefore, setting the values of $B^2$ we can construct the phase diagram in the $D$-$A$ plane.

## §5. T-P Phase Diagram for TMATC-Zn

In order to construct the $D$-$A$ phase diagram for TMATC-Zn, we must choose values of the parameters $Q$, $Q_L$ and $\epsilon_{m/l}$ for each $C_{m/l}$ phase; in this case for $m/l = \frac{1}{3}$ and $\frac{2}{5}$. In practice, such a choice have to be realized via a best fit of the theoretical T-P diagram, as obtained from the $D$-$A$ diagram, to the experimental T-P diagram shown in Fig. 2. We choose the following values of the parameters

$$Q = \frac{1}{2}, \quad Q_L^2 = \frac{1}{2}, \quad \epsilon_6 = 1, \quad \epsilon_{10} = 1. \tag{29}$$

They are taken with accuracy only up to the first digit. Figure 3 shows the $D$-$A$ phase diagram constructed according to the expressions (17)-(28) and (29). The $C_{m/l}$ phases are labeled with their ratios $m/l$. LT denotes the LT-point with its coordinates given by (27).

When constructing the T-P phase diagram from the $D$-$A$ diagram given by Fig. 3, we assume that $D$ and $A$ depend linearly on T and P. Then the T and P axes will be straight lines in the $D$-$A$ diagram. Their position, orientation, and scale are determined from the best fit to the experimental T-P diagram (Fig. 2). For simplicity we put $\tan\widehat{TD} = \tan\widehat{PA} = 2$, while the origin of theT and P axes is so chosen that they cut equal lengthes on the $D$ and $A$ axes (measureing from the LT point).

Figure 4 shows the T-P phase diagram constructed from Fig. 3 with the choice of T and P axes indicated there. The $C_{m/l}$ phases with $m/l = \frac{1}{3}$ and $\frac{2}{5}$ are hatched. The T-axis in the $D$-$A$ diagram in Fig. 3 is chosen in such a way that the $C_{m/l}$ phases intersected by the T-axis are the same and have approximately the same widths as in Fig. 2. The P-axis in the $D$-$A$ diagram in Fig. 3 is chosen

in such a way that the $C_0$-IC phase transition line has approximately the same inclination as in Fig. 2. By comparing Fig. 4 with Fig. 2, we see that the theoretical and experimental T-P phase diagrams agree sufficiently well. This agreement could be improved by making a more suitable selection of the parameters $Q$, $Q_L$ and $\epsilon_{2l}$, and by achieving a more precise orientations of the T- and P-axes in the $D$-$A$ diagram.

## §6. Discussion

In conclusion, we enumerate again all approximations and assumptions made when constructing the theoretical $D$-$A$ and T-P phase diagrams. The triple point existing in the experimental T-P diagrams for TMATC-$M$ crystal family (Figs. 1 and 2) is assumed to be the Lifshitz -type point, which was introduced in ref. 11. Owing to this assumption we succeeded in explanation of such a special feature of the diagrams as the absence of the IC phase to the left from the triple point, where the line of phase transitions separates the $C_0$ and $C_{0/1}$ phases.

The single-harmonic approximation was used for the IC phase. This leads to insignificant errors when determining the boundaries between the IC and $C_{m/l}$ phases. The weak anisotropy condition was used for the $C_{m/l}$ phases. This allows to obtain explicit expressions for the potentials, and hence, for the boundaries of the $C_{m/l}$ phases. However, for small $l$ and in a region of large $A$-values in the $D$-$A$ diagram this condition may not be well satisfied.

Construction of the phase diagram in the $D$-$A$ plane means that only $D$ and $A$ vary with T and P, while the remaining quantities are assumed to be constant. These are the $Q_L$ and $\epsilon_{2l}$ and, hence, the coefficients $\kappa$, $\tau$, $\beta$ and $\alpha'_{2l}$. The assumption that $D$ and $A$ depend linearly on T and P is valid not too far from the axes $A$ and $D$ in the $D$-$A$ diagram. When constructing the phase diagrams the numerical values of the parameters were taken with accuracy only up to the first digit.

The approximations and assumptions above-listed did not prevent us from obtaining a fairly good agreement between the theoretical and experimental T-P phase diagrams for TMATC-Zn. And this is in spite of the fact that in the phenomenological model considered here the number of dimensionless parameters which are used is small: $Q_L$ and just one parameter $\epsilon_{2l}$ for each commensurate phase. The phenomenological approach to structural phase transitions is known to be well justified. The result above mentioned demonstrates that it is just as well justified in this case, i.e., as applied to complicated phase diagrams on which the special triple point, incommensurate phase, and a large number of commensurate phases exist. This approach is considered to be adequate to the experimental data.

---


1) J. D. Axe, M. Iizumi and G. Shirane: *Incommensurate Phases in Dielectrics 2*, ed. R. Blinc and A. P. Levanyuk, (North Holland, Amsterdam, 1985) Chap.10.

2) K. Gesi: Ferroelectrics **66** (1986) 269.

3) H. Z. Cummins: Phys. Reports. **185** (1990) 211.

4) H. Shimizu, A. Oguri, N. Abe, N. Yasuda, S. Fujimoto, S. Sawada Y. Shiroishi and M. Takashige: Solid State Commun. **29** (1979) 125.
5) H. Shimizu, N. Kokubo, N. Yasuda, S. Fujimoto: J. Phys. Soc. Jpn. **49** (1980) 223.
6) S. Tanisaki and H. Mashiyama: J. Phys. Soc. Jpn. **48** (1980) 339.
7) H. Mashiyama and S. Tanisaki: Phys. Lett **76A** (1980) 347.
8) S. Yonekawa, H. Mashiyama and S. Tanisaki: J. Phys. Soc. Jpn. **55** (1986) 431.
9) H. Mashiyama: J. Phys. Soc. Jpn. **49** (1980) 2270.
10) D. G. Sannikov: Kristallografiya **36** (1991) 813. [ Sov. Phys. Crystallogr. **36** (1991) 455.]
11) T. A. Aslanyan, A. P. Levanyuk: Fiz. Tverd. Tela (Leningrad) **20** (1978) 804. [ Sov. Phys. Solid State **20** (1978) 466.]
12) R. M. Hornreich, M. Luban, S. Strikman: Phys. Rev. Lett. **35** (1975) 1678.
13) D. G. Sannikov: Kristallografiya **41** (1996) 5. [Crystallography Reports **41** (1996) 1.]
14) D. G. Sannikov: Zh. Eksp. Teor. Fiz. **96** (1989) 2189. [ Sov. Phys. JETP **69** (1989) 70.]
15) A. P. Levanyuk and D. G. Sannikov: Fiz. Tverd. Tela (Leningrad) **18** (1976) 1976. [ Sov. Phys. Solid State **18** (1976) 1122.]

Table I. The space groups of all possible commensurate phases associated with a soft optical branch with the wave vector $k_z = qc^*$ of the space group $Pmcn(D_{2h}^{16})$ of TMATC-Zn.

| $\frac{0}{1}$ | | $\frac{m_-}{l_-}$ | $\frac{m_+}{l_-}$ | $\frac{m_-}{l_+}$ |
|---|---|---|---|---|
| $P12_1/c1\ C_{2h}^5\ B_{2g}\ (zx)$ | $c_1$ | $P2_12_12_1\ D_2^4\ (xyz)$ | $P12_1/c1\ C_{2h}^5\ (zx)$ | $Pc2_1n\ C_{2v}^9\ (y)$ |
| | $c_2$ | $P112_1/n\ C_{2h}^5\ (xy)$ | $P2_1cn\ C_{2v}^9\ (x)$ | $P2_1/c11\ C_{2h}^5\ (yz)$ |
| | $c_3$ | $P112_1\ C_2^2$ | $P1c1\ C_s^2$ | $Pc11\ C_s^2$ |

Fig. 1. Unified temperature-pressure phase diagram for TMATC-$M$ family crystals from ref. 2. The position of zero pressure for each compound is plotted by an arrow. Small letter $d$ indicates the deuterated compound.

Fig. 2. The experimental T-P phase diagram for TMATC-Zn from ref. 8.

Fig. 3. The D-A phase diagram with the LT-point plotted for TMATC-Zn.

Fig. 4. The theoretical T-P phase diagram plotted on the basis of Fig. 3 for TMATC-Zn.

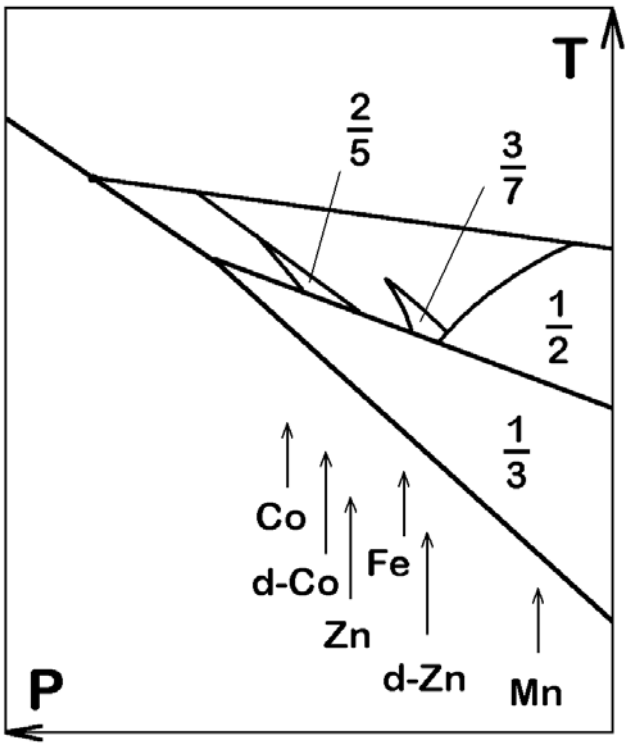


**Fig. 1..**

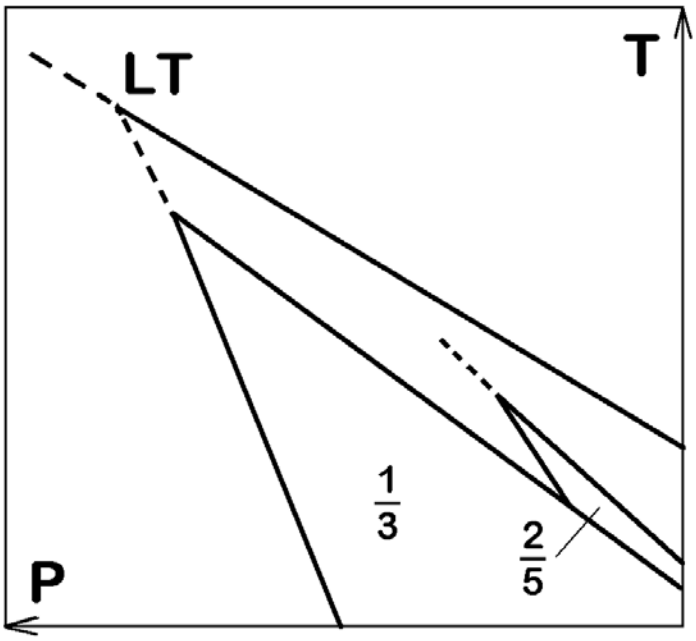


**Fig. 2.**

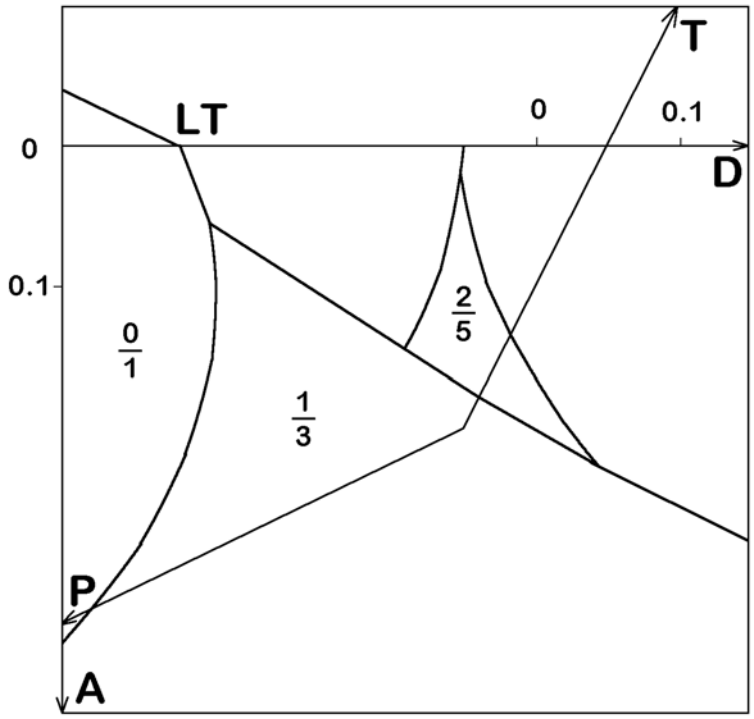


**Fig. 3.**

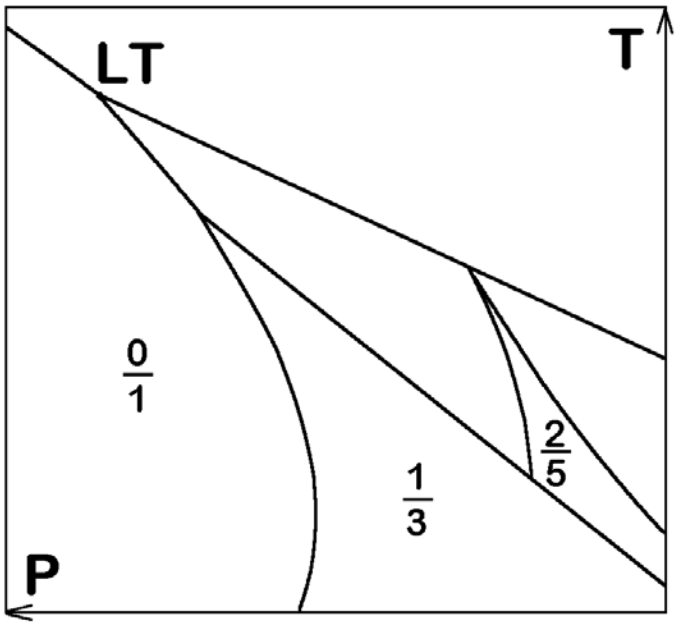


**Fig. 4.**